THE STRUCTURE OF PARAMYOSIN FIBRILS ACCORDING TO X-RAY DIFFRACTION*

BY RICHARD S. BEAR, PH.D., AND CECILY CANNAN SELBY,‡ PH.D.

(From the Department of Biology, Massachusetts Institute of Technology, Cambridge)

(Received for publication, October 6, 1955)

INTRODUCTION

Some time ago two types of fibrous component of muscles were briefly compared by means of x-ray diffraction (Bear, 1945). One of these components was originally designated type I, since it was the first to be detected by means of small-angle x-ray diffraction (Bear, 1944 *b*) and electron microscopy (Hall, Jakus, and Schmitt, 1945). Later it was given the name paramyosin, because its properties appeared to differ from those of other more widely encountered fibrous muscle constituents (Schmitt, Bear, Hall, and Jakus, 1947). Paramyosin has thus far been found only in invertebrate, mostly molluscan, muscles.

The physiological function of paramyosin is as yet uncertain, but its structure is of interest in connection with muscle problems. Not only is it present in high proportions in certain muscles, but also it yields diffraction patterns of a kind similar to, although distinctly different from, a major one more commonly observed in muscles (type II of Bear, 1945), considered further in the immediately following paper.

In the original x-ray study of paramyosin (Bear, 1944 *b*) complete resolution of diffracted spots was not obtained on a single pattern, but conclusions were reached by a combination of pinhole- with slit-collimated photographs. The former furnished imperfect resolution transverse to the fiber axis, while the latter yielded adequate resolution in a direction paralleling the fiber axis. Since then, technical improvements of pinhole cameras have produced patterns which resolve, in single photographs, all spots of appreciable intensity and add a few new ones. This paper describes the new patterns and considers their significance.

Experimental Methods

The diffraction cameras used at wide diffraction angles were the moderately finely collimated ones briefly described by Bear (1944 *a*), but those employed at small diffraction angles were the improved models of Bolduan and Bear (1949), in particular those designated

* This investigation was supported in part by Research Grant C-1780 from the National Cancer Institute of the National Institutes of Health, Public Health Service.

‡ Present address: Department of Anatomy, Cornell University Medical College, New York.

as having resolution (*fd*) of 400 and 800 A. Ni-filtered radiation from commercial Cu-target x-ray tubes was directed through specimens of about 1 mm. thickness toward flat films (Eastman type K) located 3 to 5 cm. from the specimen in wide-angle observation or 15 cm. for the small-angle studies. Exposure times ranged from a day or two for wide-angle patterns (showing also incompletely resolved small-angle spots; see Fig. 1), to as much as about 300 hours for the pinhole patterns of greatest resolution (see Fig. 2), with tube loading 18 to 20 ma. at about 35 k.v.p. Small-angle cameras were evacuated with a mechanical pump during exposure.

Muscle specimens in general diffract relatively weakly, in comparison to other protein fibers, and it is particularly difficult to examine them at small-angles when they are diluted by their normal complements of water. The most complete diagrams for paramyosin were obtained with specimens which had finally been dried in a vacuum oven before insertion in the evacuated cameras. Some indications of the effects of swelling were obtained by adding water to previously dried specimens after these had been introduced into thin walled pyrex capillaries, which were finally sealed in a flame to prevent drying during radiation. This method made easier the preservation of orientation in the pliable wet specimens.

Although various molluscan sources have been used, the preferable one for paramyosin is the "white" portion of the adductor muscle of *Venus mercenaria* because of the high content of paramyosin (*cf.* Bear, 1945; Schmitt, Bear, Hall, and Jakus, 1947). The small-angle pattern is then only weakly overlaid with the type II (actin) diffraction.

Orientation of fibrous structure is most easily preserved during drying by allowing strips of appropriate diameter to remain *in situ* between intact upper and lower shells of the clam (excess clam body and muscle is removed through apertures made by cutting away portions of the shell). The shells may be allowed to open and stretch the muscle strips as much as 30 % beyond normal closed shell length before diffraction deteriorates due to slipping or tearing within the muscle. This degree of elongation, and indeed even comparable contraction, does not result in spacing changes or alteration of spot relative intensities, although the moderately elongated specimens are best for orientation.

The attached strips were dried at room temperature, with a current of air directed around and through the shells, and then removed. Paramyosin fibrils are relatively stable: reasonable modifications of drying rates and temperatures, as well as lengthy storage in the dried condition, did not noticeably influence diffraction results.

RESULTS

Fig. 1 shows a wide-angle pattern of a specimen which exhibited centrally very little evidence of anything but paramyosin. The wide-angle equatorial and meridional arcs are those expected of KMEF fibers of α-type, although close inspection shows the features specific for the clam muscles, as drawn and described by Bear (1944 *b*). White *Venus* muscle manifestly contains a high proportion of paramyosin, so that it is highly probable that paramyosin belongs to the α-KMEF class of proteins and thus may have fine structure similar to hair keratin and the myosin component of vertebrate muscles. Since the small-angle reflections described below show no appreciable arcing, the fibrils of the specimens were well oriented and the peculiar shape of the equatorial diffraction must be due largely to intrafibrillar structure, plus the effects of inherent rotation about the oriented fibrillar axis.

Of greater concern to the present discussion is the small-angle pattern shown in Fig. 2, which is the best one obtained. Close inspection discloses that this

pattern, while symmetrical across the meridian and approximately centrosymmetrical, is more clearly developed above the equator. This results from the fact that the muscle fiber was tilted slightly (less than one degree) so that its axis departed from orthogonality to the x-ray beam. Under this condition the reciprocal structure above the equatorial plane is tilted into the sphere of reflection, while that below the equatorial plane is correspondingly tilted out of the sphere. Accordingly, the upper half of the pattern presents the better section through the reciprocal structure, particularly for the higher layer lines, and the pattern thus obtained is more satisfactory for analysis than are ones secured from untilted specimens.

All the diffractions which escape the heavy central diffuse scatter lie on three types of vertical row line: (1) the central meridional line ($h = 0$) of strongest spots, which occur at horizontal layer lines whose indices (k) are multiples of 5; (2) the moderately strong pairs of spots forming vertical rows ($h = \pm 1$) to either side of the meridian and confined to adjacent layer lines midway between those whose k indices are multiples of 5; and (3) two faint spots represented by observable diffraction at the 6th and 19th layer lines, where intensity occurs at transverse locations corresponding, as nearly as can be judged, to index assignment $h = \pm 2$.

Fig. 3 shows the central small-angle diffraction of a rehydrated specimen. In this case fewer layers of high k index were obtained, but three new reflections at lower layers ($k = 1$, 2, and 3) were observed. These were found at transverse locations suggesting h indices of -2, $+1$, and -1, respectively, according to the interpretation presented below.

Examination of Fig. 2 shows that on the $h = \pm 1$ row lines, at each pair of vertically adjacent reflections the one with the lesser k index is slightly further removed from the meridian than is its mate on the next higher layer. Furthermore, when the transverse locations of all $h = \pm 1$ reflections are examined in detail (see Fig. 4) one discovers that within experimental error they lie on two slightly curved row lines which cross at the equator. This behavior is expected of row lines $+h$ and $-h$ which (a) are superimposed by the natural rotation of fibrils about their long axes within the fibrous specimen, (b) are nonorthogonal to the equatorial plane of reciprocal space, and (c) are composed of reflections sharp enough to make the curvature of the sphere of reflection apparent.

Under these conditions (also at very small diffraction angles and with slight tilt of the fiber axis) the rotation-diagram coordinates of Bernal (1926) are found from the approximate relations:

$$\zeta^2 - X^2 \doteq \frac{Y^2}{4} \frac{(2\theta - Y)^2}{(1 - C)^2}$$

and

$$\zeta \doteq Y.$$

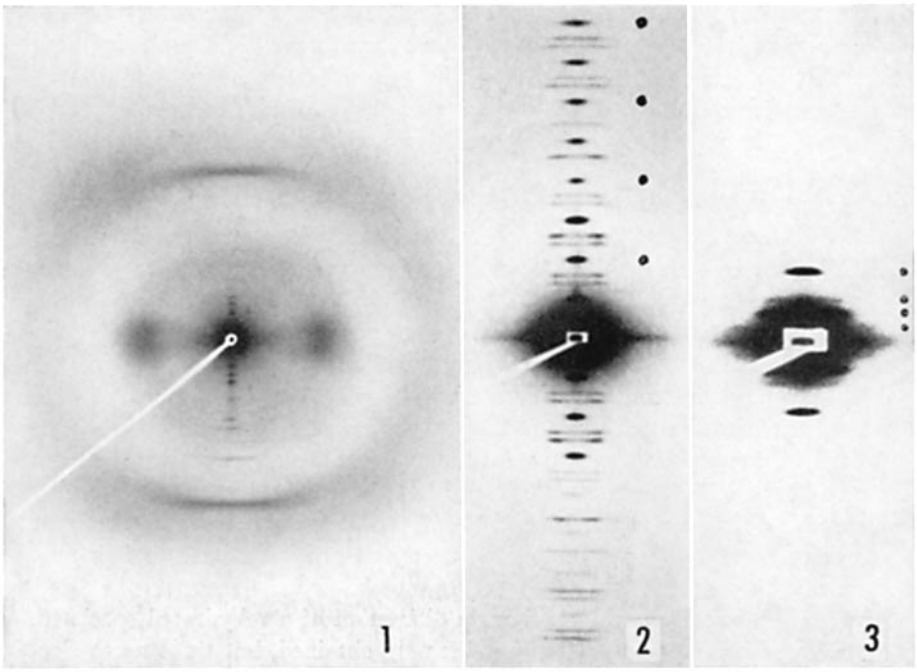

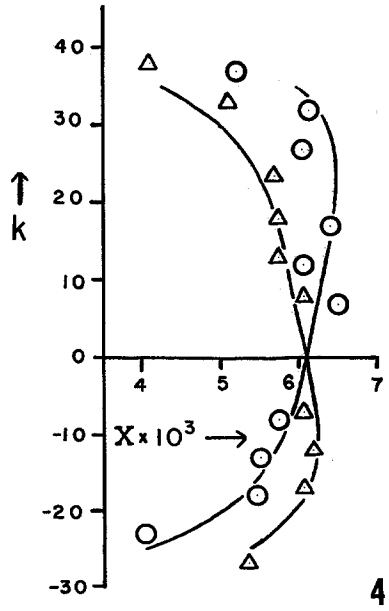

4

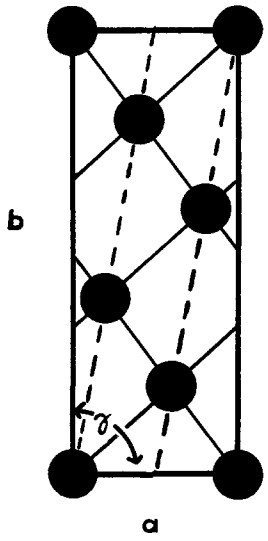

5

Here ξ and ζ are the *corrected* Bernal reciprocal space coordinates, transverse to and along the rotation (or fiber) axis, respectively, and X and Y are *observed* angular transverse and vertical locations of the reflections on the pattern (Fig. 2). The tilt, θ, is the very small angle that the specimen's fiber axis departs from normality to the x-ray beam. The quantity C is essentially a transverse half-breadth of the reflections (expressed as a fractional part of average X), which causes them to close into the meridian, because of tilt and reflection-sphere curvature, under conditions at which very narrow reflections ($C = 0$) would remain separate.

In applying these corrections to the paramyosin case, the parameters θ and C were selected to straighten the row lines, and they were found to be, for the pattern of Fig. 2: $\theta = 0.013$ radian (or 0.74°) and $C = 0.45$. These values could be seen by inspection of the pattern to be reasonable. In Fig. 4 calculated and observed positions for the reflections of Fig. 2 are compared.

Corrections of this sort are, however, negligible for the central reflections, *i.e.* those on layer lines between $k = -8$ to $+18$, hence the corrections do not influence conclusions regarding the dimensions and angles of the net cell deduced below. The corrections were studied for reassurance that the features causing row-line crossing and curvature were understood. Table I presents the final rotation-diagram coordinates, also averaged for the information gained from upper and lower halves of the diagram. The possibility of distinction of the two branches of the $h = \pm 1$ row line permitted assignment of arbitrary signs to these indices, but the $h = \pm 2$ reflection are too few and widely spaced to permit sign distinction experimentally. In these cases assignment of sign was made on the basis of the selection rules discussed below.

Note that only the index set (hk) is needed to describe all the observed small-angle reflections of paramyosin. The simplest interpretation of the diagram is, therefore, that it arises from a two dimensionally periodic assembly of equiva-

---

FIG. 1. Wide-angle diffraction pattern of dry, white *Venus* adductor muscle. The relatively diffuse diffraction, characterized chiefly by the intense arcs on the equator (horizontal midline) and meridian (vertical midline) is typical of α-type fibrous proteins. The crowded reflections close to the meridian centrally are the ones seen at greater magnification in Fig. 2.

FIG. 2. Small-angle diffraction pattern ot the above specimen at the same orientation. Dots along the upper half of the diagram indicate k levels which are multiples of 10. The meridional reflections ($h = 0$) are strongest, and the crossed row lines ($h = \pm 1$), further described in the text, are to either side.

FIG. 3. Small-angle diffraction by a rehydrated specimen of the same muscle. Dots mark levels of reflections at $k = 1, 2, 3$, and 5, reading upward.

FIG. 4. Curvature of the $h = \pm 1$ row lines shown by exaggeration of the observed transverse coordinates (X) relative to the k-level scale. Circles and triangles indicate the actually measured positions (on Fig. 2) of reflections belonging to the respective $+1$ and -1 branches. Curves indicate theoretical shapes for the branches according to equations and constants described in the text.

FIG. 5. The paramyosin net cell. The magnitudes of the elements a, b, and γ are described in the text. Solid circles denote nodes, whose primitive connection is shown by light continuous lines; the outline of the non-primitive cell is heavy. Dashed lines show the nodal connection preferred for the supercabled "rods" in the Discussion section.

lent scatterers, *i.e.* the paramyosin fibril is basically a large-scale net of material which periodically repeats itself along the fibril axis and in one dimension transverse thereto. Diffraction from the other transverse direction has escaped

TABLE I

Small-Angle Diffraction of Dry Paramyosin

k	ζ ($\times 10^2$)	h	ξ ($\times 10^2$)	I
5	1.08	0	—	*vs*
6	1.26	(−)2	(12.3)	*vw*
7	1.51	+1	6.3	*m*
8	1.71	−1	5.9	*m*
10	2.16	0	—	*vs*
12	2.58	+1	6.3	*m*
13	2.80	−1	5.7	*m*
15	3.21	0	—	*vs*
17	3.68	+1	6.4	*w*
18	3.88	−1	5.8	*w*
19	4.05	(+)2	(13.0)	*vw*
20	4.27	0	—	*s*
23	4.97	−1	5.5	*m*
25	5.17	0	—	*s*
27	5.83	+1	6.6	*w*
30	6.42	0	—	*s*
32	6.78	+1	(6.6)	*m*
33	7.03	−1	(5.8)	*w*
35	7.51	0	—	*s*
37	7.90	+1	(6.4)	*m*
38	8.19	−1	(5.8)	*m*
40	8.60	0	—	*s*

The second and fourth columns express (in radians) the vertical and horizontal rotation-diagram coordinates of the reflections of Fig. 2. Where possible, values given are averages of data from upper and lower halves of the pattern. The ξ values are corrected for tilt and reflection sphere curvature as described in the text. Parentheses enclose less reliable ξ estimates. First and third columns show indexing appropriate for the reflections as observed in the upper right quadrant of the pattern. Magnitudes of h are determined by location relative to the pattern meridian, and the crossed row lines ($h = \pm 1$) are arbitrarily distinguished by opposite signs of h. This choice determines the right-left orientation of the net cell in Fig. 5. Parentheses enclose h values whose sign is suggested by the selection rule of the text. The last column indicates reflection intensities as *vs*, *s*, *m*, *w*, *vw* in order of decreasing strength.

attention thus far, or it is possible that in this third direction the fibrils are too thin, too poorly ordered, or of too short periodicity to be apparent at small diffraction angles, except in influence on spot extension transverse to the fibril axis (*cf.* Bear and Bolduan, 1950 *a*).

The present observations, in terms of locations of intensity maxima as given in Table I, permit construction of the net cell shown in Fig. 5. The average value

of the periodicity, b, along the fibril axis (derived from the relations $b = k\lambda/\zeta$ for all reflections) is 720 ± 5 A for dry paramyosin. Inclinations of the $h = \pm 1$ row lines to the equator show the angle between cell edges to depart from orthogonality by about 0.5°; *i.e.*, $\gamma = 90.5 \pm 0.2°$. The a cell dimension is 250 ± 10 A.

For rehydrated material measurements of ζ coordinates for lines with $k =$ 1, 2, 3, 5, 7, 10, and 13 yielded $b = 725 \pm 5$ A, indicating no certain change in this cell dimension during swelling. Estimates of a and γ for the moist state depend on ξ coordinates of the reflections at $k = 1, 2, 3$, which are difficult to estimate accurately because of interference of central scatter. It seemed clear that a increases considerably to 325 ± 20 A, while γ increases somewhat further from orthogonal, during swelling. All reflections of moist material occurred satisfactorily close to transverse locations required by the selection rule discussed below.

The solid circles (nodes) in Fig. 5 indicate distribution of centers of nearly equivalent x-ray scattering power (*i.e.* similar structure) over the net cells. Their location is determined by the fact that all observed paramyosin reflections follow the selection rule:

$$h = \frac{k - 5m}{2},$$

in which m is any positive or negative integer, including zero. The many other (hk) choices possible for the same net with nodes solely at corners are not observed.

This selection rule is easily derived from the transform (unitary structure factor) for such a net cell, which is proportional to:

$$T(hk) = \sum_j \exp\,[2\pi i(hu_j + kv_j)].$$

Here u_j and v_j are coordinates of the jth node in fractions of the a and b cell edges, respectively, and summation is over the 5 nodes of a cell. For this operation it is convenient to choose 5 nodes in a row, with coordinates $u_j = -2j/5$, $v_j = j/5$, as is permissible because corresponding nodes of adjacent cells scatter alike to all diffraction maxima. Evaluation of the transform yields:

$$T(hk) = \sum_{j=0}^{4} \exp\left[\frac{2\pi ij}{5}(-2h + k)\right]$$

$$= \frac{\exp\,[2\pi i(-2h + k)] - 1}{\exp\left[\frac{2\pi i}{5}(-2h + k)\right] - 1}.$$

Scattering intensity is large at those reflections (hk) whose transform is large, *i.e.* whose denominator above is zero, as happens when the selection rule above is fulfilled. The selection rule can be expressed in other equivalent forms but is here stated in a manner convenient for the discussion of the net-helix ambiguity below.

The patterns show other scattering effects at central areas, as can be seen on Fig. 2. These include (*a*) a diffuse blackening within angles corresponding to Bragg spacings of about 100 A, possibly arising from more or less globular particulate matter of muscle; (*b*) a very diffuse circular halo, which is poorly oriented equatorially and corresponds to a spacing of roughly 60 A, a reasonable value for lipid contaminants; and (*c*) a well oriented equatorial streak extending out to about the location of the halo, indicating the presence of independently scattering, thin elements of thickness approximating 40 to 60 A.

The relation of these effects to the paramyosin component is doubtful, with the possible exception of (*c*), and they have not been investigated in detail during this study. Scattering components (*a*) and (*b*) interfere with registration of paramyosin layer lines below $k = 5$ with dry specimens, but addition of water has permitted penetration through some of the central fog.

DISCUSSION

The Paramyosin Net

The diffraction data presented herein for paramyosin add the following extensions to the earlier information (Bear, 1944 *b*): (*a*) transverse parameters of the structure are better determined, although some discrepancy between x-ray and electron-optical results remains (see below); (*b*) the two branches of the $h = \pm 1$ row line have been distinguished, with the result that it has become possible to offer an analysis of structure from the x-ray data alone (at least as far as the net description); and (*c*) all observed reflections, which occur at k indices from 1 to 40 and h indices from 0 to 2, are now in agreement with the postulated net cell.[1]

The determination of ξ as well as ζ coordinates, and of the relative signs of $h = \pm 1$ reflections, has permitted more precise statement of the selection rule. This selection rule was anticipated in the early observations (Bear, 1944 *b*), before its cause could be stated, and now is seen to follow from the peculiar type of non-primitive net cell which is most conveniently chosen for the paramyosin fibril. If, instead of using the non-primitive cell, one adopts a primitive cell covering one-fifth the former's area and with smaller cell edges, the new axes of reference have no simple relation to the important fibril axis. For this reason the non-primitive choice is more significant.

Earlier electron-optical studies of Hall, Jakus, and Schmitt (1945) also resulted in postulation of a two dimensionally ordered construction for paramyosin fibrils. The cell of the net as determined thereby had $a = 193$ A, $b = 725$ A, $\gamma = 90°$, in close agreement with the x-ray cell relative to the identity

[1] Certain of the faint lines reported from the early slit-camera photographs (Table III of Bear, 1944 *b*; k indices 9, 11, 21, 34, and 36) have not been observed on the present pinhole photographs. While the revised selection rule allows them to be present at $h = \pm 2$, and they might be expected to appear with the normally more intense registration secured by slit collimation, the earlier failure to find similar reflections at $k = 6$ and 19, as now observed, suggests that the previous report was in error because of illusory appearances attending observation of a series of otherwise equally spaced lines.

period along with fibril axis. The number and manner of distribution of nodes were also the same as proposed here. Chief differences are noticed in the size of the a translation and the non-orthogonality of the γ angle.

If the electron-optically derived cell be regarded as that of a thoroughly dehydrated specimen, then there is a progression of a and γ values from the electron-optical cell, through the dry x-ray specimen's cell, to the deliberately hydrated situation. However, the dry specimen for x-rays had been oven-dried and remained in a roughly evacuated camera (use of glass capillaries was not adopted in this case to avoid absorption losses of x-ray intensity). Although it may have regained some moisture over the extended photographic exposure, one experiences difficulty in believing that the a cell dimension for the two dry specimens could differ so greatly in fact. Possibly the electron-optical and diffraction methods do not view the same projection of the net's a translation. Further examination will be required before the causes of the discrepancy can be established.

The electron-optical evidence indicated that total fibrillar width in the net plane, parallel to the a cell edge, is that of from 1 to about 5 net cells (up to 1000 A), while net cells are repeated many b translations along the fibril axis (*ca.* 600b in 40 μ fibrils of maximum length). No reliable electron-optical estimates are available, however, for the thickness of isolated fibrils normal to the ordered net plane.

We have attempted to estimate this third dimension from densitometer determination of transverse lengths of meridional reflections. This involved complex theoretical and experimental operations (see Cannan, 1950) which will not be detailed here. Theoretical expressions were developed for diffraction shapes expected of very long, two dimensionally ordered fibrils, having finite transverse (ordered and non-ordered) dimensions. Allowance was made for the appreciable divergence of the incident beam, for the non-parallelism of row lines with the pattern meridian, and for rotation of the fibrils of the specimen about the fiber axis. Electron-optical estimates of prevalent fibril width in the ordered transverse dimension were also employed. The conclusion was that the x-ray specimens contained fibrils of about 500 A thickness normal to the net plane; *i.e.*, the native fibrils are of the same degree of thickness in both ordered and non-ordered transverse dimensions.

Isolated fibrils as observed electron-optically often seem to have a flattened ribbon-like appearance, but this may result from longitudinal cleavage brought about by the physical and chemical maceration used in preparing them for examination. Examination of thin cross-sectional slices of the clam adductor muscle has not revealed paramyosin fibrils of pronounced ribbon-like section (*cf.* Fig. 5 of Hodge, Huxley, and Spiro, 1954), although intrafibrillar filaments show a greater tendency to be arranged in sheets than to exhibit the hexagonal packing often observed in sections of striated muscle (Selby, 1953). This question is worthy of further electron-optical study.

Macromolecular Structure

If the paramyosin wide-angle diagram is of α-type, as seems highly probable, then according to current conceptions of the interpretation of α-diagrams (Pauling and Corey, 1953; Crick, 1953), one must assume that in paramyosin

fibrils there are cables[2] of supercoiled α-helices of diameter about 30 A. Hodge (1952) has, in fact, isolated and characterized physicochemically elements approximately of this diameter and of length about 1000 to 1500 A. These he could reconstitute into symmetrical, smoothly cross-striated ribbons of axial periodicity averaging near 1400 A, as seen electron-optically.

Taking this last figure as a more reliable value for particle lengths than the physicochemical measurements provide, one can calculate that this length of α-helix (at 1.5 A axial projection per residue) should have weight of about 100,000. Hodge found that the dispersed particles are fairly homogeneous and have weights of several hundred thousand in acid solutions (pH 3.5) of ionic strength near or above 0.1. These sizes are consistent with cables formed by twisting together several coils. From acid solution at higher ionic strength the reconstituted ribbons appear, but at lower ionic strength particle dissociation occurs, including the release of a second component of much lower particle weight. Pauling and Corey have indicated that supercoiled aggregates would require several components to secure good packing and utilization of available space.

Hodge did not discover conditions for reconstitution of the native variety of net-like fibril under present discussion. However, his results did suggest a tendency of the particles to unite in sheet-like structures of 40 to 100 A thickness, rather than in the hexagonal type of packing that is normally expected.

The constancy of the axial period (b) in the paramyosin net during swelling, in contrast to the highly variable a cell width, indicates that long, thin elements (rods) constitute the net and would lie along the b axis or at a small angle thereto. It is important to realize that there is nothing in the net cell description that tells how the nodes may be connected by these rods, although one would expect that they might lie parallel to, or effectively along, lines connecting nodes.

There are two nodal connections which seem reasonable in the light of the facts considered above. In the first, the rods would follow nodal connection paralleling the b axis, which would permit a single cable within the rod, of *ca.* 1400 A length, to run through two nodes along two net cells. During swelling adjacent rods thus aligned would be displaced slightly along the b axis relative to each other, in order to cause the angle γ to depart from 90°.

[2] Hierarchies of subfibrillar element are indicated herein as follows: A ***helix*** or ***coil*** (when applied to residue scale structure) is a helically wound molecular chain, in this case an α-helix. A ***cable*** consists of several helices whose separate axes are coiled (the helices are then ***supercoiled***) about the cable axis. Likewise, a ***supercable*** contains several cables whose individual axes are further twisted about the supercable axis. The term ***particle*** is used in a general sense and does not imply by itself any particular shape or internal structure. ***Rod*** is employed to distinguish the total, very asymmetric aggregate of molecular chains which, whatever the internal configuration, interconnects net nodes; in the proposed paramyosin structure ***rods*** are believed to be ***supercables***.

A second type of connection would place the rods along the internodal connection shown as dashed lines in Fig. 5. Each cable in a rod would extend over two cells and connect five nodes. This connection has the property that only displacements normal to the rod axes are needed to account for variations in γ during swelling.

One can estimate rod diameter from the space available to each across the net. For the case of nodal connection along the fibril axis, five rods would lie side-by-side across the a cell dimension; rod diameter is thus 40 to 50 A, depending on whether electron-optical or x-ray measurements of a are adopted for dry material. For the second choice, with inclination (10°) of rods to the fibril axis, the a translation comprises approximately two rod diameters, which are, accordingly, 100 to 125 A each in the dry state. Note that in this case the indicated rod diameters are great enough to permit formation of supercables, from, for example, such elements as the Pauling-Corey seven strand cables, which have individual diameters of *ca.* 30 A.

Some preferences for the second type of connection can be derived from the general distribution of diffracted intensity about the pattern meridian.[3] A single solid rod of 100 A diameter would scatter most strongly to positions within row lines $h = \pm 3$, as is observed. On the other hand, rods of 40 to 50 A diameter should scatter strongly as far out as the row lines $h = \pm 6$ to 8, as is not observed. Placing the rods into a net merely causes "sampling" of the single rod scatter, according to the nature of the net, in a manner described in development of the selection rule above.

With either of the nodal connections the crystallography of the situation makes a further demand of the supercabled rods. Each node must have about it similar structure. Thus, the 1400 A cables must have internal structure repeated two or five times along each, or the several cables must be aggregated in such a way that indefinitely long rods are formed with identical structure repeated at the internodal distance along them. Details of this sort cannot, of course, be proposed with certainty at this stage, but are outlined here as examples of the requirements imposed upon model construction by the diffraction data.

Presumably the net-like sheets of rods described above are stacked normal to their faces to form the total paramyosin fibril of the tissue. Each sheet would be minimally of thickness approximating that of rod diameters (100 A). Intersheet separations of this size have not thus far been apparent on the x-ray patterns, but they would occur centrally on the equator at a region which has not as yet been exhaustively examined and which presents technical difficulties because of diffuse central scatter.

[3] This argument is based on the fact that the transform at all layer lines for a rod with periodic structure along its axis is proportional to $2J_1(x)/x$, in which $x = \pi D\xi/\lambda$, D is the rod diameter, ξ is the variable expressing angle of scatter transverse to the rod axis, and λ is the wave length of the radiation (Bear and Bolduan, 1950 *b*). The row-line positions cited correspond to the first zero of the first-order Bessel function, J_1.

The Net-Helix Ambiguity

The probable importance of the ordered large-scale net in paramyosin was appreciated as early as the studies of Hall, Jakus, and Schmitt (1945). Later Cochran, Crick, and Vand (1952) described how helical assemblages of matter should diffract, and it became quickly apparent that helical structures provided an alternative way to interpret the selection rule exhibited by paramyosin diffractions. These authors showed that the relation,

$$\frac{n}{P} + \frac{m}{p} = \frac{k}{b},$$

existed between integral indices n, m, and k, determining the distribution of diffracted intensity; P, the pitch of the helix; and p, the axial projection per individual, of the helically arranged, equivalently scattering units (nodes) of matter. These units and the pitch periodically repeat the structure over intervals of length b along the axis. A simple rearrangement derives

$$n = \frac{k - mM}{N_0},$$

in which $M = b/p$, the number of equivalent units per identity, b, and $N_0 = b/P$, the number of helical turns per identity. Comparison with the net selection rule given above for paramyosin shows that if $M = 5$, $N_0 = 2$, n is used instead of h, and k and m retain their former significance, the two equations become identical.

The index n, like h, determines lateral location of diffraction maxima relative to the pattern meridian (n's are the orders of Bessel functions describing the diffraction). Within the accuracy with which paramyosin diffraction positions and shapes can be measured it would be possible to interpret the paramyosin pattern in terms of helices with 5 equivalent scattering units arranged in 2 helical turns along 725 A of fibril axis.[4]

The helix which would be thus derived is one of helically arranged large particles, like those envisaged by Pauling (1953), rather than of smaller atom groups or residues, as in the α-helix. The reason for the formal similarity of planar-net and helix diffraction is easily seen from Fig. 5. If, for example, the net cell is multiplied many times along b, and then the assembly is rolled cylindrically so that the vertical edges coincide, one obtains a helical arrangement of nodes.

The helix-net and planar-net transverse cell dimensions, derivable from the same data interpreted in the two ways, are not identical, however. For example, the transverse cell edge for the helix-net is πD, in which D is the di-

[4] This is actually a description of the *genetic* helical arrangement in the sense described by Bear (1955). Here, as also in the net description above, there remain ambiguities of nodal connection.

ameter of the cylindrical shell upon which nodal centers occur.[5] The diameter for the large-scale paramyosin helix would be 150 A for the dry x-ray specimen.

It is also possible to explain the paramyosin diffractions in terms of helices made by approximately doubling, trebling, *etc.*, the helix diameter and correspondingly increasing the circumferential number of the helix-net cells used in forming the helix (*cf.* the discussion of "net ambiguities" of helices by Bear, 1955).

The possibility of analysis of small-angle paramyosin diffraction in helical terms is worth the attention given above, both because this type of paradox arises in other situations—wherever, in fact, either true planar-net or helix diffraction is encountered—and because it could happen that future data regarding paramyosin may favor the helical interpretation, though this does not appear likely at the moment.

Perhaps the primary reason for doubting the helical choice is derived from the electron-optical data. Hall, Jakus, and Schmitt (1945) believed they could discard the possibility that the fibrils might be flattened cylindrical objects. A flattened helix should appear the same from any side, but enantiomorphic paramyosin fibrils have been observed in single electron-micrograph fields, as would be expected from the random turning over of true nets (Hall, private communication). An unflattened helix viewed from the side should *not* show, in projection, the distribution of nodes that is seen electron-optically.

Another reason for preference of the planar-net is that the crossed row lines ($h = \pm 1$) are thereby more directly and simply interpreted. It would seem a remarkable fortuity that the distribution of electron density radially in a helical structure should be just that to simulate the crossing of row lines observed.

The cable-like units derived above from Hodge's work can be fitted somewhat more reasonably into the planar-net than into the possible helix-net models. While we have described the rod-like elements of the proposed planar-net model to be in fact supercables of coiled coils, the diffraction selection rules for such cases (Crick, 1953) are more complicated than is observed for paramyosin. Actually, compactly wound supercables of this kind might be expected to scatter x-rays at small angles much like solid rods, and the discontinuities determining diffraction may well be merely the troughs and crests of electron density at locations

[5] D is determinable from the positions for maxima of $J_n^2(\pi D\xi_n/\lambda)$, in which ξ_n is the rotation-diagram coordinate for an intensity maximum ascribed to the Bessel function term J_n, whose argument is in parentheses. For the truly planar net, maxima occur on layer lines at $\xi_n = h\lambda/a$ (here the slight inclination of row lines is neglected). For n or h unity, as on the major paramyosin row lines, and letting $\xi_n = \xi_h$ to obtain the relation between D and the planar-net's transverse cell dimension, we have

$$\frac{\pi D}{a} = 1.84$$

or

$$D = 0.586a.$$

The factor 1.84 is the value of J_1's argument at the first maximum.

of rod or cable boundaries, of molecular chain terminations, of heavy or light side chains, or of packing difficulties of the latter. If these density variations are spatially distributed over planes the planar-net type of diffraction might well predominate at small angles.

SUMMARY

From analysis of x-ray diffraction patterns obtained with improved small-angle techniques has been derived the following description for the structure of the fibrils of the fibrous protein, paramyosin, obtained in this case from "white" portions of the adductor muscle of the clam, *Venus mercenaria*:

1. About 25 significantly different diffraction maxima have been resolved and found accounted for as (*hk*) reflections of a net whose cell elements are, for the dry material: $a = 250$ A, $b = 720$ A (fibril axis identity period), and $\gamma = 90.5°$ (angle included between a and b axes). For rehydrated material a is larger (*ca.* 325 A), b is essentially unchanged, and γ is slightly larger. There remains an unresolved discrepancy between the electron-optically derived cell's a dimension (193 A) and that here reported for dry samples.

2. The $h = \pm 1$ row lines are crossed on the diagrams (because γ is not 90°) and thus can be distinguished in spite of natural "rotation" of fibrils (within the massive fibrous specimens) about their commonly oriented axes. The observed reflections are then found to obey a selection rule which indicates that the net cell is non-primitive and contains 5 equivalent locations (nodes) arranged as shown in Fig. 5. The nodal distribution is the same as has been previously photographed electron-optically.

3. Analysis of reflection lengths indicates that the native fibrils are not noticeably ribbon-like, having dimensions normal to the ordered net layers approximating their width across the fibril in the plane of the net layers. Corresponding transverse, interlayer spacings (possibly *ca.* 100 A) have not been observed, however, and may be hidden in troublesome central scatter.

4. Since paramyosin's wide-angle diffraction is very probably of α-type, supercoiled α-helices must be involved according to current interpretations of α-diagrams. Physicochemical evidence suggests that cables of this type, *ca.* 1400 A in length, may extend over two cells. Of two possible nodal connections, a favored one is shown in Fig. 5 to join 5 nodes in this way. Considerations of space filling, of transverse distribution of small-angle x-ray scattering, and of nodal significance, suggest that the cable units may be further aggregated into supercables, essentially forming rather solid rods of *ca.* 100 A diameter.

5. An alternative interpretation of the paramyosin small-angle diffraction, in particular of the observed selection rule, would conclude that large particles are arranged in a helical way, with minimum helix diameter about 150 A (dry). The simplest (genetic) particle connection would have 5 particles in 2 coil turns along 720 A of fibril or helix axis. This view is distinctly different from the

arrangement of "rods" in net-like layers as given above, even though the rods are said to be made of supercoils or cables. Reasons are given for preferring the net-of-rods explanation over the particulate-helix model. The helix- *vs.* true-net ambiguity arises whenever the two types of structure are conceivable, and decision between them is difficult on the basis of the diffraction data alone.

REFERENCES

Bear, R. S., *J. Am. Chem. Soc.*, 1944 *a*, **66**, 1297.
Bear, R. S., *J. Am. Chem. Soc.*, 1944 *b*, **66**, 2043.
Bear, R. S., *J. Am. Chem. Soc.*, 1945, **67**, 1625.
Bear, R. S., *Symp. Soc. Exp. Biol.* (*Great Britain*), 1955, No. 9, 97.
Bear, R. S., and Bolduan, O. E. A., *Acta Cryst.*, 1950 *a*, **3**, 230.
Bear, R. S., and Bolduan, O. E. A., *Acta Cryst.*, 1950 *b*, **3**, 236.
Bernal, J. D., *Proc. Roy. Soc. London, Series A.*, 1926, **113**, 123.
Bolduan, O. E. A., and Bear, R. S., *J. Appl. Physics*, 1949, **20**, 983.
Cannan, C. M. M., An X-Ray Diffraction Investigation of the Ultrastructure of Muscle, Ph.D. Thesis, Massachusetts Institute of Technology Library, Cambridge, 1950. All experimental material presented herein is derived from this thesis, which was prepared during the author's tenure of a United States Public Health Service Fellowship.
Cochran, W., Crick, F. H. C., and Vand, V., *Acta Cryst.*, 1952, **5**, 581.
Crick, F. H. C., *Acta Cryst.*, 1953 *a*, **6**, 685.
Crick, F. H. C., *Acta Cryst.*, 1953 *b*, **6**, 689.
Hall, C. E., Jakus, M. A., and Schmitt, F. O., *J. Appl. Physics*, 1945, **16**, 459.
Hodge, A. J., *Proc. Nat. Acad. Sc.*, 1952, **38**, 850.
Hodge, A. J., Huxley, H. E., and Spiro, D., *J. Exp. Med.*, 1954, **99**, 201.
Pauling, L., *Discussions Faraday Soc.*, 1953, No. 13, 170.
Pauling, L., and Corey, R. B., *Nature*, 1953, **171**, 59.
Schmitt, F. O., Bear, R. S., Hall, C. E., and Jakus, M. A., *Ann. New York Acad. Sc.*, 1947, **47**, 799.
Selby, C. C., *Cancer Research*, 1953, **13**, 753.